

Proposal for asymmetric photoemission and tunneling spectroscopies in Fermi-Hubbard model on triangular optical lattices

Shuai A. Chen,¹ Qianqian Chen,² and Zheng Zhu^{2,3,*}

¹*Department of Physics, Hong Kong University of Science and Technology, Clear Water Bay, Hong Kong, China*

²*Kavli Institute for Theoretical Sciences, University of Chinese Academy of Sciences, Beijing 100190, China*

³*CAS Center for Excellence in Topological Quantum Computation,
University of Chinese Academy of Sciences, Beijing, 100190, China*

(Dated: February 15, 2022)

Recent realization of well-controlled triangular optical lattices loaded with ultracold Fermions and the more advanced techniques to probe it pave the way for studying frustrated Fermi-Hubbard physics. Here, we theoretically predict asymmetric photoemission and tunneling spectroscopies for a lightly hole-doped and electron-doped triangular Mott antiferromagnet, and reveal two distinct types of magnetic polarons: a *lightly* renormalized quasiparticle with the same momentum as the spin background and a *heavily* renormalized quasiparticle with a shifted momentum and a nearly flat band, using both analytical and unbiased numerical methods. We propose these theoretical findings to be verified in frustrated optical lattices and Moiré superlattices by probing various observables including the spectral function, the density of states, the energy dispersion and the quasi-particle weight. Moreover, we reveal the asymmetric response of the spin background against charge doping, demonstrating that the interplay between the local spin and charge degrees of freedom plays a vital role in doped triangular Mott antiferromagnets.

Introduction.— The Fermi-Hubbard model is widely believed to be a prototypical model to capture the essential physics of many realistic strongly correlated systems, notably the doped Mott insulators [1]. Important insights into the doped Mott insulators could be gained by investigating the motion of the doped single charge and its interplay with the spin background. Due to its potential relevance to the high T_c cuprates [2, 3], such an issue has been extensively studied on the square lattice [4]. Nevertheless, those analogous problems on the triangular lattice, which are equally important and likely to exhibit distinct physics due to the geometric frustrations and the absence of particle-hole symmetry, still need plenty of endeavors.

Recently, quantum simulating the Fermi-Hubbard model has been realized in both cold-atom optical lattices [5–25] and condensed-matter Moiré superlattices [26, 27], and the theoretical predictions can thereby be verified. Compared with the complicated condensed-matter materials [26, 27], a more controlled pristine optical lattice has been remarkably advanced [5–25], where the momentum-resolved spin structure factor [20], the spectral function [23, 24] and the real-space motion of the doped hole [21, 22] can be probed using high-resolution techniques. In particular, more recently, the triangular optical lattice loaded with ultracold Fermions has been implemented experimentally [11], as illustrated in Fig. 1(a), the coupling strength U and the hopping amplitude t could be accurately tuned through Feshbach resonance [28] and the strength of the optical lattice [25], respectively. With the revolutionary real-space detection using quantum gas microscopy [5], the dynamics of all ultracold atoms can be imaged simultaneously, making it possible to precisely track the motion of a single charge in a background of fluctuating spins [21, 22]. Moreover, the interplay between charge and spins is also encoded in the spectral function, which is readily obtained in optical lattice via angle-resolved photoemission spectroscopy (ARPES)

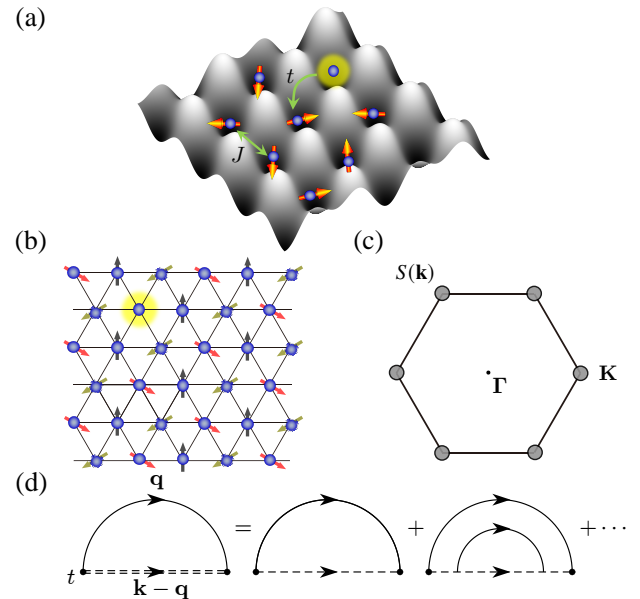


Fig. 1. (Color online.) (a) Fermions trapped in a triangular optical lattice. A 120° antiferromagnetic order emerges with a characteristic energy scale J , and it further dresses a bare hole with a cloud of magnons. (b) Schematic diagram of triangular Mott antiferromagnet with a single doped charge. (c) Schematic diagram of the static spin structure factor $S(\mathbf{k})$ for the 120° Néel order at half filling. The maxima of $S(\mathbf{k})$ are denoted by solid gray circles. (d) The rainbow diagram for SCBA calculations. Holon and magnon are presented by solid and dashed lines, respectively. The double dashed line represents the exact holon propagator. The vertex marked by the black dot is of order t .

[23, 24] that measures the quasiparticle with energy and momentum resolution.

Motivated by the above aspects, in this Letter, we propose the photoemission and tunneling spectroscopies of a single

charge doped triangular Mott antiferromagnet in optical lattices. By establishing the magnetic polaron theory and adopting self-consistent Born approximation (SCBA), we theoretically predict asymmetric photoemission and tunneling spectroscopies and identify two distinct types of magnetic polarons: a lightly renormalized quasiparticle with the same momentum as the spin background and a heavily renormalized quasiparticle with a shifted momentum and nearly flat band. Interestingly, the latter case provides a new way to engineer the topology and Kondo physics in doped Mott insulators. The density matrix renormalization group (DMRG) simulation backs up the analytical conclusions. We further show the asymmetric responses of the spin background against charge doping concentration and demonstrate the validity of our theory at light doping. We remark that the signature of the asymmetry proposed here, including the spectral function, the density of states, and the static spin structure factor, can be directly probed in recently realized frustrated optical lattices.

Model Hamiltonian.— The motion of the doped charge in a triangular optical lattice [11] can be described by the Fermion-Hubbard model

$$H = -t \sum_{\langle ij \rangle \sigma} (c_{i\sigma}^\dagger c_{j\sigma} + h.c.) + \frac{U}{2} \sum_i (n_i - 1)^2, \quad (1)$$

where $c_{i\sigma}^\dagger$ ($c_{i\sigma}$) and n_i denote a fermion creation (annihilation) and particle number operators at site i , respectively. The summation runs over all the nearest-neighbor links $\langle ij \rangle$. In this work, we focus on the strong coupling regime, where the Hamiltonian at half-filling reduces to a pure Heisenberg spin model with the superexchange coupling $J = 4t^2/U$ and 120° Néel order in the ground state [29–32]. Upon doping a charge, i.e., $\sum_i n_i = N - 1$ (N the number of the lattice sites), the hopping process is triggered with amplitude t . Then the low-energy effective Hamiltonian reads

$$H = -t\mathcal{P} \sum_{\langle ij \rangle \sigma} (c_{i\sigma}^\dagger c_{j\sigma} + h.c.)\mathcal{P} + J \sum_{\langle ij \rangle} \mathbf{S}_i \cdot \mathbf{S}_j, \quad (2)$$

where \mathcal{P} imposes no double occupancy constraint, i.e. $n_i \leq 1$. Unlike the bipartite square-lattice case [33–42], the particle-hole symmetry is absent on the non-bipartite triangular lattice, i.e., the physics depends on the sign of hopping amplitude t [43, 44]. We therefore perform a comparative study for $t > 0$ and $t < 0$, and are devoted to light doping exemplified by a single charge doping with the methods of the SCBA [35, 36, 45, 46] and DMRG [47, 48].

Magnetic polaron theory.— We start from the half-filled spin background with an in-plane order, here the 120° Néel order is characterized by momentum $\mathbf{Q} = \mathbf{K}$ for the triangular Mott antiferromagnets [29–32]. We consider the order in XZ-plane and an in-plane rotation of each spin at \mathbf{r}_i by an angle $\mathbf{Q} \cdot \mathbf{r}_i$. Implementing the Holstein-Primakov transformation with $S_i^z = S - a_i^\dagger a_i$, $S_i^+ = a_i$, we introduce a boson a to describe the low-energy magnon excitations and get the Hamiltonian $H_a = \sum_{\mathbf{k}} \omega_{\mathbf{k}}^s \beta_{\mathbf{k}}^\dagger \beta_{\mathbf{k}}$, where $\omega_{\mathbf{k}}^s =$

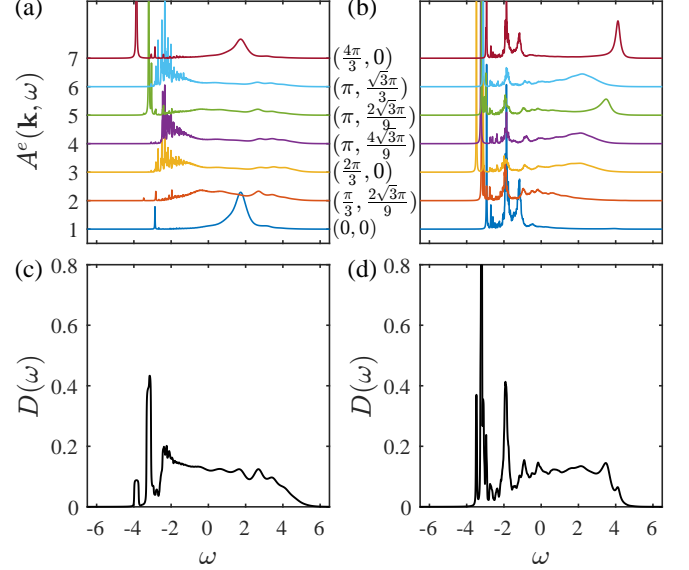


Fig. 2. (Color online.) The spectral function $A^e(\mathbf{k}, \omega)$ [(a) and (b)] and density of states $D(\omega)$ [(c) and (d)] obtained from SCBA at $N = 6 \times 6$ lattice with periodic boundary conditions. A well-defined quasiparticle peak lies at the bottom of spectrum with $\mathbf{K} = (\frac{4\pi}{3}, 0)$ for $t/J = 5$ in (a) and $(\frac{2\pi}{3}, 0)$ for $t/J = -5$ in (b), respectively. The density of states $D(\omega)$ features a vanishing gap in a continuum limit for both sides, and for $t/J = -5$ in (d), it shows the divergent Van Hove singularity behavior. Here we set $|t| = 1$ as the unity of energy, and $\delta = 0.01$.

$\frac{\nu}{2} JS \sqrt{(1 - \gamma_{\mathbf{k}})(1 + 2\gamma_{\mathbf{k}})}$ denotes the energy dispersion of magnons and the canonical modes $\beta_{\mathbf{k}} = u_{\mathbf{k}} a_{\mathbf{k}} - v_{\mathbf{k}} a_{-\mathbf{k}}^\dagger$. Here $\gamma_{\mathbf{k}} = \sum_{\delta} e^{i\mathbf{k} \cdot \delta} / \nu$ sums over all $\nu = 6$ nearest-neighbor sites on triangular lattice and $u_{\mathbf{k}}, v_{\mathbf{k}}$ are usual Bogoliubov factors in spin-wave theory. Then the rotated ground state can be constructed as $|\Psi_0\rangle = \exp(-\sum_{\mathbf{k}} \frac{v_{\mathbf{k}}}{u_{\mathbf{k}}} a_{\mathbf{k}} a_{-\mathbf{k}}) |\text{N\'eel}\rangle$.

Upon doping, the motion of the charge is dressed by magnons, forming a magnetic polaron. The creation of a spinless charge is described by h_i^\dagger in the fractionalization scheme: $c_{i\uparrow} = h_i^\dagger$ and $c_{i\downarrow} = h_i^\dagger S_i^+ = h_i^\dagger a_i^\dagger$. Ignoring higher-order interactions, we derive the effective Hamiltonian with two terms: the kinetic energy term

$$H_{h0} = - \sum_{\mathbf{k}} \omega_0^h(\mathbf{k}) h_{\mathbf{k}} h_{\mathbf{k}}^\dagger \quad (3)$$

with dispersion relation $\omega_0^h(\mathbf{k}) = \frac{\nu t}{2} (\gamma_{\mathbf{k}+\frac{\mathbf{Q}}{2}} + \gamma_{\mathbf{k}-\frac{\mathbf{Q}}{2}})$ and the holon-magnon coupling term

$$H_{hb} = - \frac{\nu t}{i\sqrt{N}} \sum_{\mathbf{k}, \mathbf{q}} h_{\mathbf{k}} h_{\mathbf{k}-\mathbf{q}}^\dagger (M_{\mathbf{k}} a_{\mathbf{q}}^\dagger - M_{\mathbf{k}-\mathbf{q}} a_{-\mathbf{q}}) \quad (4)$$

with $M_{\mathbf{k}} = \gamma_{\mathbf{k}+\frac{\mathbf{Q}}{2}} - \gamma_{\mathbf{k}-\frac{\mathbf{Q}}{2}}$, which describes the motion of the charge in the process of absorbing or emitting magnons. We remark that, in sharp contrast to the triangular-lattice case, the kinetic energy term of the magnetic polarons is absent in

the square-lattice case [35, 36]. To obtain the single-particle Green's function $G^h(\mathbf{k}, \omega) \equiv \langle \Psi_0 | h_{\mathbf{k}} \frac{1}{\omega - H} h_{\mathbf{k}}^\dagger | \Psi_0 \rangle$, we adopt the SCBA, i.e., considering the rainbow Feynman diagrams sketched in Fig. 1(d), to get the self energy

$$\Sigma^h(\mathbf{k}, \omega) = \sum_{\mathbf{q}} \frac{f(\mathbf{k}, \mathbf{q})}{\omega - \omega_0^h(\mathbf{k} - \mathbf{q}) - \omega_{\mathbf{q}}^s - \Sigma^h(\mathbf{k} - \mathbf{q}, \omega - \omega_{\mathbf{q}}^s)},$$

where $f(\mathbf{k}, \mathbf{q}) = (\nu t)^2 |M_{\mathbf{k}} v_{\mathbf{q}} - M_{\mathbf{k}-\mathbf{q}} u_{\mathbf{q}}|^2 / N$ denotes the vertex coupling originated from holon-magnon interaction.

Photoemission and Tunneling Spectroscopies.— To directly compare with the experiments, we compute the Green's function $G^e(\mathbf{k}, \omega)$ that connects to $G^h(\mathbf{k}, \omega)$ via the relation

$$G^e(\mathbf{k}, \omega) = -\frac{1}{4} G^h(\mathbf{k} + \frac{\mathbf{Q}}{2}, \omega) - \frac{1}{4} G^h(\mathbf{k} - \frac{\mathbf{Q}}{2}, \omega). \quad (5)$$

The momentum shift $\pm \mathbf{Q}/2$ is induced by the rotation on $|\Psi_0\rangle$, and for triangular Mott antiferromagnets, $\mathbf{Q} = \mathbf{K}$. Below we show the spectral function $A^e(\mathbf{k}, \omega)$ and the density of states $D(\omega)$, both of which are experimentally detectable through the ARPES [23, 24] and scanning tunneling microscope (STM).

The spectral functions $A^e(\mathbf{k}, \omega) \equiv \frac{1}{\pi} \text{Im} G^e(\mathbf{k}, \omega + i\delta)$ are presented in Figs. 2(a-b) for $t/J = \pm 5$ on a $N = 6 \times 6$ lattice with energy resolution δ . We have confirmed their robustness on larger size with the convergence guaranteed by energy resolution $\delta = 0.01$. For $t/J = 5$, as shown in Fig. 2(a), we find that, in the spectral function, the sharp peak at momentum $\mathbf{K} = (\frac{4\pi}{3}, 0)$ with the lowest energy signals a well defined quasiparticle, which separates from the peaks at other momenta with higher energy. Interestingly, unlike the square-lattice case, where the 180° Néel order and the doped hole locate at momenta (π, π) and $(\pi/2, \pi/2)$, respectively, here the momentum of the doped charge is the same as that of the spin background with 120° Néel order. However, for $t/J = -5$, although we can still identify a well-defined quasiparticle peak at momentum $(\frac{2\pi}{3}, 0)$, there are numerous excitations with a fairly close energy scale, as demonstrated in Fig. 2(b), suggesting a heavily reduced bandwidth compared with the $t/J = 5$ side. This observation demonstrates that the doped charge is highly renormalized with much larger effective mass and much smaller quasiparticle weight. Notably, we can observe some Lorentz-like broadening peaks at much higher energies with momenta $(\frac{4\pi}{3}, 0)$ and $(0, 0)$, which reflects the spin dynamics and confirms our theoretical setup.

Moreover, we compute the density of states $D(\omega) = \sum_{\mathbf{k}} A^e(\mathbf{k}, \omega)$ that can be directly probed by an STM experiment. As shown in Fig. 2(c), we find $D(\omega)$ characterizes a well-defined quasiparticle at $t/J > 0$ side. However, for $t/J < 0$ shown in Fig. 2(d), the divergence of $D(\omega)$ near the ground state signals the Van Hove singularity behavior or the nearly flat band, suggesting the numerous excitations near the ground state [see Fig. 2(b)], consistent with many low-energy peaks in a narrow energy window in the spectral functions $A^e(\mathbf{k}, \omega)$ [see Fig. 2(b)].

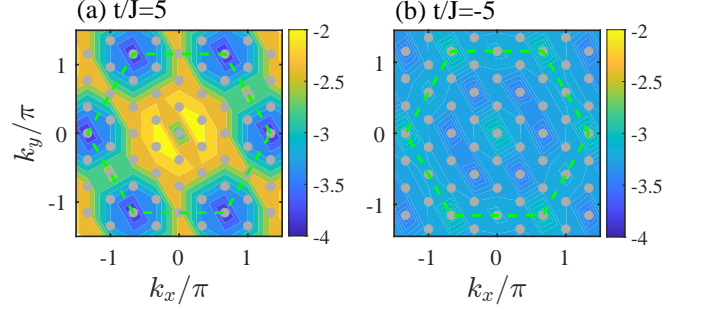


Fig. 3. (Color online.) Energy dispersion. Energy dispersion for a single charge in (a) $t/J = 5$ and (b) $t/J = -5$ from SCBA. The gray dots mark the accessible Bloch momenta on a $N = 6 \times 6$ lattice.

We remark that the asymmetric spectral functions $A^e(\mathbf{k}, \omega)$ and density of states $D(\omega)$ at both sides indicate the distinct bandwidth for the doped charge, which can be inferred from the gaps between peaks in $A^e(\mathbf{k}, \omega)$ [see Figs. 2(a) and (b)], or more clearly, from the energy dispersion $\omega^h(\mathbf{k})$ shown in Fig. 3. Within the same color scale, we can find the nearly flat band with vanishingly small bandwidth when $t/J < 0$, but a well-defined dispersive quasiparticle when $t/J > 0$. The nearly flat band implies the doped charge is heavily renormalized, giving rise to much larger effective mass or much smaller quasiparticle weight. The minimum in the energy dispersion $\omega^h(\mathbf{k})$ characterizes the ground-state momentum of the doped charge, which is also confirmed by the DMRG simulations below.

Numerical simulation.— We employ the DMRG method to confirm the ground-state momentum obtained by SCBA. Moreover, we explain the asymmetric behavior by probing the spin channel and reveal that our proposal works at light doping. For numerical simulation, it requires the integral multiple of 3 for system length L_x and width L_y in order to accommodate the 120° Néel order, and DMRG computational cost increases exponentially with L_y , we therefore primarily focus on $L_y = 6$ cylinders with the bond dimension up to $D=20,000$. The charge doping can be accurately controlled by implementing $U(1)$ symmetries.

The direct way to examine the momentum of the doped charge is to compute the quasiparticle spectral weight distribution $Z_{\mathbf{k}}$, which is defined by the overlap between the one-hole ground-state wave function $\Psi_{1\text{-hole}}$ and the wave function obtained by removing an electron from the ground state at half filling $\Psi_{0\text{-hole}}$, i.e.,

$$Z_{\mathbf{k}} \equiv |\langle \Psi_{1\text{-hole}} | c_{\mathbf{k}} | \Psi_{0\text{-hole}} \rangle|^2. \quad (6)$$

Figures 4(a) and (b) show the contour plot of $Z_{\mathbf{k}}$ for $t/J = 5$ and $t/J = -5$ with $L_y = 6$ cylinder geometry, respectively. The location of the peak in $Z_{\mathbf{k}}$ characterizes the ground-state momentum of the doped charge. For $t/J = 5$, the significant peaks at momenta \mathbf{K} suggest the well-defined quasiparticle behavior of the single charge [see Fig. 4(a)]. However, for

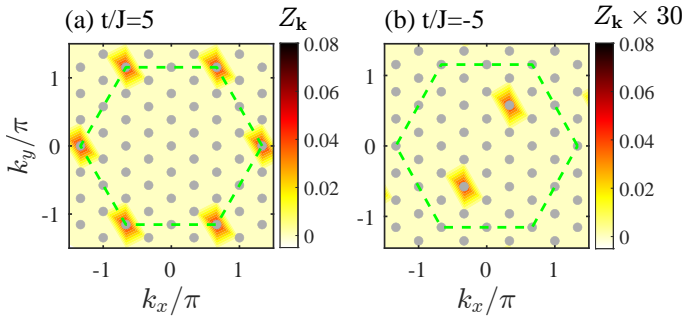


Fig. 4. (Color online). The quasiparticle spectral weight $Z_{\mathbf{k}}$ for (a) $t/J = 5$ and (b) $t/J = -5$ with a single charge doping. The gray dots represent the accessible momenta with $N = 6 \times 6$ cylinder geometry.

$t/J = -5$, we find that the peaks locate at momentum $\mathbf{K}/2$ [see Fig. 4(b)]. Particularly, $Z_{\mathbf{k}}$ at $t/J = -5$ is highly suppressed, thus we multiply it with a factor 30 to clearly compare the two sides. The locations of the peaks in $Z_{\mathbf{k}}$ from DMRG back up the SCBA results, demonstrating the magnetic polaron theory indeed captures the nature of a doped charge in the triangular-lattice antiferromagnets, although the values of $Z_{\mathbf{k}}$ are different. The distinct momenta for opposite signs of t/J also manifests the particle-hole asymmetry in the triangular lattice. Given the relation $Z_{\mathbf{k}} \sim m/m^*$, with m the bare electron mass and m^* the effective mass of quasiparticle, our results indicate that the effective mass of the doped single charge at $t/J < 0$ is much larger than $t/J > 0$, or equivalently, the band at $t/J < 0$ is quite narrow or nearly flat.

To explore the distinct behavior of the doped charges at two sides and check the validity of our magnetic polaron theory, we probe the spin channel at light dopings by computing the static spin structure factor

$$S(\mathbf{k}) = \frac{1}{N} \sum_{i,j} \langle \mathbf{S}_i \cdot \mathbf{S}_j \rangle e^{i\mathbf{k} \cdot (\mathbf{r}_i - \mathbf{r}_j)}, \quad (7)$$

which can be directly probed in an optical lattice [20]. At half filling, the 120° Néel order is characterized by the sharp peaks of $S(\mathbf{k})$ at $\mathbf{k} = \mathbf{Q}$, as is shown in Fig. 1(c). To probe the evolution of the spin background with doping, we keep track of $S(\mathbf{k} = \mathbf{Q})$ as a function of doping concentration δ , as shown in Figs. 5. For $t/J > 0$, we find the spin background is insensitive to the light doping, as indicated by the robust sharp peak of $S(\mathbf{k} = \mathbf{Q})$ for $\delta \lesssim 10\%$ [see Fig. 5 (a)]. However, the 120° Néel order is rapidly weakened at $t/J < 0$ even with a much lower doping level $\delta \lesssim 5\%$ [see Fig. 5 (b)], suggesting the motion of the charge may induce a global distortion on the spin background, which in turn would further dress the doped charge, giving rise to the significantly enhanced effective mass. The 120° Néel order is also the precondition of magnetic polaron theory, and our findings of $S(\mathbf{k})$ against doping suggest such a theory is valid at least for $\delta \lesssim 5\%$ at both sides, while for a wider range at the $t/J > 0$

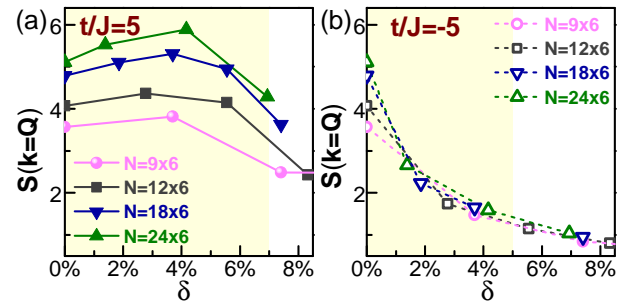


Fig. 5. (Color online). The spin structure factor $S(\mathbf{k} = \mathbf{Q})$ as a function of charge doping concentration δ for $t/J = 5$ (a) and $t/J = -5$ (b) on $L_y = 6$ cylinders.

side. The distinct nature of the ground state in both charge and spin channels exhibits the particle-hole asymmetry and reveals the intricate interplay between the charge and spin degrees of freedom.

Summary and Outlook.— In summary, we theoretically predict asymmetric photoemission and tunneling spectroscopies for the lightly doped triangular Mott antiferromagnets and identify two distinct types of magnetic polarons on frustrated lattices: the lightly renormalized quasiparticle with the same momentum as the spin background, and the heavily renormalized quasiparticle with a shifted momentum. The latter provides a new way to engineer the flat bands and explore the possible topology and Kondo physics in doped Mott insulators. We further show the asymmetric responses of the spin background against doping and confirm the validity of our theory at least within $\delta < 5\%$. Our findings might motivate future theoretical studies on the interplay between the local degrees of freedom and the geometric frustration, or on the possible emerged phases with further increased doping concentration [49], both of which are of fundamental importance for understanding the Fermi-Hubbard physics on frustrated lattices.

Moreover, the triangular-lattice Fermi-Hubbard model has recently been realized on the frustrated optical lattices [11], in which both the ratio U/t and charge doping can be accurately tuned [5–18, 25, 28], then our predictions of the spectral function and the static spin structure factor are readily verified based on recently developed techniques including ARPES [23, 24] and the coherent manipulation of spin correlations [20]. Additionally, the transition-metal dichalcogenide (TMD) and its heterostructures can also simulate the triangular-lattice Hubbard model [26, 27] with widely tunable parameters such as the ratio U/t and the charge carrier density [50–53]. Utilizing the STM and the recently developed nano-ARPES techniques [54], our predictions of the spectral function and the density of state at light doping can also be directly tested. These proposals based on our theory may also inspire more experimental ideas beyond the extensively studied square-lattice case.

We would like to thank T. K. Ng, A. Vishwanath, D. N. Sheng, J. H. Mao, Y. Xu for helpful discussions. This work was supported by the National Natural Science Foun-

dation of China (Grant No. 12074375), the Fundamental Research Funds for the Central Universities (Grant No. 2020001601), the start-up funding of KITS at UCAS (Grant No.118900M026), and the Strategic Priority Research Program of CAS (Grant No.XDB33000000).

* zhuzheng@ucas.ac.cn

- [1] P. A. Lee, N. Nagaosa, and X.-G. Wen, Doping a Mott insulator: Physics of high-temperature superconductivity, *Rev. Mod. Phys.* **78**, 17 (2006).
- [2] P. W. Anderson, The resonating valence bond state in La_2CuO_4 and superconductivity, *Science* **235**, 1196 (1987).
- [3] B. Keimer, S. A. Kivelson, M. R. Norman, S. Uchida, and J. Zaanen, From quantum matter to high-temperature superconductivity in copper oxides, *Nature* **518**, 179 (2015).
- [4] E. Dagotto, Correlated electrons in high-temperature superconductors, *Rev. Mod. Phys.* **66**, 763 (1994).
- [5] C. Gross and W. S. Bakr, Quantum gas microscopy for single atom and spin detection, *Nature Physics* (2021).
- [6] A. Bohrdt, L. Homeier, C. Reinmoser, E. Demler, and F. Grusdt, Exploration of doped quantum magnets with ultracold atoms, *Annals of Physics* **435**, 168651 (2021), special issue on Philip W. Anderson.
- [7] W. S. Bakr, J. I. Gillen, A. Peng, S. Fölling, and M. Greiner, A quantum gas microscope for detecting single atoms in a Hubbard-regime optical lattice, *Nature* **462**, 74 (2009).
- [8] M. F. Parsons, A. Mazurenko, C. S. Chiu, G. Ji, D. Greif, and M. Greiner, Site-resolved measurement of the spin-correlation function in the Fermi-Hubbard model, *Science* **353**, 1253 (2016).
- [9] J. F. Sherson, C. Weitenberg, M. Endres, M. Cheneau, I. Bloch, and S. Kuhr, Single-atom-resolved fluorescence imaging of an atomic Mott insulator, *Nature* **467**, 68 (2010).
- [10] L. W. Cheuk, M. A. Nichols, K. R. Lawrence, M. Okan, H. Zhang, E. Khatami, N. Trivedi, T. Paiva, M. Rigol, and M. W. Zwierlein, Observation of spatial charge and spin correlations in the 2D Fermi-Hubbard model, *Science* **353**, 1260 (2016).
- [11] J. Yang, L. Liu, J. Mongkolkiattichai, and P. Schauss, Site-resolved imaging of ultracold fermions in a triangular-lattice quantum gas microscope, *PRX Quantum* **2**, 020344 (2021).
- [12] F. Schäfer, T. Fukuhara, S. Sugawa, Y. Takasu, and Y. Takahashi, Tools for quantum simulation with ultracold atoms in optical lattices, *Nature Reviews Physics* **2**, 411 (2020).
- [13] M. Boll, T. A. Hilker, G. Salomon, A. Omran, J. Nespolo, L. Pollet, I. Bloch, and C. Gross, Spin- and density-resolved microscopy of antiferromagnetic correlations in Fermi-Hubbard chains, *Science* **353**, 1257 (2016).
- [14] P. T. Brown, D. Mitra, E. Guardado-Sánchez, P. Schauß, S. S. Kondov, E. Khatami, T. Paiva, N. Trivedi, D. A. Huse, and W. S. Bakr, Spin-imbalance in a 2D Fermi-Hubbard system, *Science* **357**, 1385 (2017).
- [15] P. T. Brown, D. Mitra, E. Guardado-Sánchez, R. Nourafkan, A. Reymbaut, C.-D. Hébert, S. Bergeron, A.-M. S. Tremblay, J. Kokalj, D. A. Huse, P. Schauß, and W. S. Bakr, Bad metallic transport in a cold atom Fermi-Hubbard system, *Science* **363**, 379 (2019).
- [16] E. Guardado-Sánchez, A. Morningstar, B. M. Spar, P. T. Brown, D. A. Huse, and W. S. Bakr, Subdiffusion and heat transport in a tilted two-dimensional Fermi-Hubbard system, *Phys. Rev. X* **10**, 011042 (2020).
- [17] J. Koepsell, S. Hirthe, D. Bourgund, P. Sompel, J. Vijayan, G. Salomon, C. Gross, and I. Bloch, Robust bilayer charge pumping for spin- and density-resolved quantum gas microscopy, *Phys. Rev. Lett.* **125**, 010403 (2020).
- [18] T. Hartke, B. Oreg, N. Jia, and M. Zwierlein, Doublon-hole correlations and fluctuation thermometry in a Fermi-Hubbard gas, *Phys. Rev. Lett.* **125**, 113601 (2020).
- [19] I. Bloch, J. Dalibard, and S. Nascimbene, Quantum simulations with ultracold quantum gases, *Nature Physics* **8**, 267 (2012).
- [20] N. Wurz, C. F. Chan, M. Gall, J. H. Drewes, E. Cocchi, L. A. Miller, D. Pertot, F. Brennecke, and M. Köhl, Coherent manipulation of spin correlations in the Hubbard model, *Phys. Rev. A* **97**, 051602 (2018).
- [21] C. S. Chiu, G. Ji, A. Bohrdt, M. Xu, M. Knap, E. Demler, F. Grusdt, M. Greiner, and D. Greif, String patterns in the doped Hubbard model, *Science* **365**, 251 (2019).
- [22] J. Koepsell, J. Vijayan, P. Sompel, F. Grusdt, T. A. Hilker, E. Demler, G. Salomon, I. Bloch, and C. Gross, Imaging magnetic polarons in the doped Fermi-Hubbard model, *Nature* **572**, 358 (2019).
- [23] P. T. Brown, E. Guardado-Sánchez, B. M. Spar, E. W. Huang, T. P. Devereaux, and W. S. Bakr, Angle-resolved photoemission spectroscopy of a Fermi-Hubbard system, *Nature Physics* **16**, 26 (2020).
- [24] A. Bohrdt, D. Greif, E. Demler, M. Knap, and F. Grusdt, Angle-resolved photoemission spectroscopy with quantum gas microscopes, *Phys. Rev. B* **97**, 125117 (2018).
- [25] M. Lewenstein, A. Sanpera, and V. Ahufinger, *Ultracold Atoms in Optical Lattices: Simulating quantum many-body systems* (Oxford University Press, 2012).
- [26] Y. Tang, L. Li, T. Li, Y. Xu, S. Liu, K. Barmak, K. Watanabe, T. Taniguchi, A. H. MacDonald, J. Shan, *et al.*, Simulation of Hubbard model physics in WSe_2/WS_2 moiré superlattices, *Nature* **579**, 353 (2020).
- [27] D. M. Kennes, M. Claassen, L. Xian, A. Georges, A. J. Millis, J. Hone, C. R. Dean, D. Basov, A. N. Pasupathy, and A. Rubio, Moiré heterostructures as a condensed-matter quantum simulator, *Nature Physics* **17**, 155 (2021).
- [28] C. Chin, R. Grimm, P. Julienne, and E. Tiesinga, Feshbach resonances in ultracold gases, *Rev. Mod. Phys.* **82**, 1225 (2010).
- [29] S. Sachdev, Kagomé- and triangular-lattice heisenberg antiferromagnets: Ordering from quantum fluctuations and quantum-disordered ground states with unconfined bosonic spinons, *Phys. Rev. B* **45**, 12377 (1992).
- [30] F. Wang and A. Vishwanath, Spin-liquid states on the triangular and Kagomé lattices: A projective-symmetry-group analysis of schwinger boson states, *Phys. Rev. B* **74**, 174423 (2006).
- [31] A. L. Chernyshev and M. E. Zhitomirsky, Spin waves in a triangular lattice antiferromagnet: Decays, spectrum renormalization, and singularities, *Phys. Rev. B* **79**, 144416 (2009).
- [32] X.-Y. Song, C. Wang, A. Vishwanath, and Y.-C. He, Unifying description of competing orders in two-dimensional quantum magnets, *Nature communications* **10**, 1 (2019).
- [33] W. F. Brinkman and T. M. Rice, Single-particle excitations in magnetic insulators, *Phys. Rev. B* **2**, 1324 (1970).
- [34] B. I. Shraiman and E. D. Siggia, Mobile vacancies in a quantum heisenberg antiferromagnet, *Phys. Rev. Lett.* **61**, 467 (1988).
- [35] C. L. Kane, P. A. Lee, and N. Read, Motion of a single hole in a quantum antiferromagnet, *Phys. Rev. B* **39**, 6880 (1989).
- [36] G. Martinez and P. Horsch, Spin polarons in the t - J model, *Phys. Rev. B* **44**, 317 (1991).
- [37] Z. Zhu, H.-C. Jiang, Y. Qi, C. Tian, and Z.-Y. Weng, Strong correlation induced charge localization in antiferromagnets, *Scien-*

- tific reports **3**, 1 (2013).
- [38] Z. Zhu, H.-C. Jiang, D.-N. Sheng, and Z.-Y. Weng, Nature of strong hole pairing in doped Mott antiferromagnets, *Scientific reports* **4**, 1 (2014).
- [39] S. Chen, Q.-R. Wang, Y. Qi, D. N. Sheng, and Z.-Y. Weng, Single-hole wave function in two dimensions: A case study of the doped Mott insulator, *Phys. Rev. B* **99**, 205128 (2019).
- [40] J.-Y. Zhao, S. A. Chen, H.-K. Zhang, and Z.-Y. Weng, Two-hole ground state: Dichotomy in pairing symmetry, *arXiv preprint arXiv:2106.14898* (2021).
- [41] A. Bohrdt, E. Demler, F. Pollmann, M. Knap, and F. Grusdt, Parton theory of angle-resolved photoemission spectroscopy spectra in antiferromagnetic Mott insulators, *Phys. Rev. B* **102**, 035139 (2020).
- [42] A. Bohrdt, E. Demler, and F. Grusdt, Rotational resonances and regge-like trajectories in lightly doped antiferromagnets, *Phys. Rev. Lett.* **127**, 197004 (2021).
- [43] Y. Krockenberger, I. Fritsch, G. Cristiani, A. Matveev, L. Alff, H.-U. Habermeier, and B. Keimer, Epitaxial growth of Na_xCoO_2 thin films by pulsed-laser deposition, *Applied Physics Letters* **86**, 191913 (2005).
- [44] Q.-H. Wang, D.-H. Lee, and P. A. Lee, Doped t - J model on a triangular lattice: Possible application to $\text{Na}_x\text{CoO}_2 \cdot y\text{H}_2\text{O}$ and $\text{Na}_{1-x}\text{TiO}_2$, *Phys. Rev. B* **69**, 092504 (2004).
- [45] M. Vojta, Spin polarons in triangular antiferromagnets, *Phys. Rev. B* **59**, 6027 (1999).
- [46] A. E. Trumper, C. J. Gazza, and L. O. Manuel, Quasiparticle vanishing driven by geometrical frustration, *Phys. Rev. B* **69**, 184407 (2004).
- [47] S. R. White, Density matrix formulation for quantum renormalization groups, *Phys. Rev. Lett.* **69**, 2863 (1992).
- [48] S. Östlund and S. Rommer, Thermodynamic limit of density matrix renormalization, *Phys. Rev. Lett.* **75**, 3537 (1995).
- [49] Z. Zhu, D. Sheng, and A. Vishwanath, Doped mott insulators in the triangular lattice hubbard model, *arXiv preprint arXiv:2007.11963* (2020).
- [50] Y. Pan, S. Fölsch, Y. Nie, D. Waters, Y.-C. Lin, B. Jariwala, K. Zhang, K. Cho, J. A. Robinson, and R. M. Feenstra, Quantum-confined electronic states arising from the moiré pattern of MoS_2 – WSe_2 heterobilayers, *Nano letters* **18**, 1849 (2018).
- [51] L. Wang, E.-M. Shih, A. Ghiotto, L. Xian, D. A. Rhodes, C. Tan, M. Claassen, D. M. Kennes, Y. Bai, B. Kim, *et al.*, Correlated electronic phases in twisted bilayer transition metal dichalcogenides, *Nature materials* **19**, 861 (2020).
- [52] E. C. Regan, D. Wang, C. Jin, M. I. B. Utama, B. Gao, X. Wei, S. Zhao, W. Zhao, Z. Zhang, K. Yumigeta, *et al.*, Mott and generalized wigner crystal states in WSe_2 / WS_2 moiré superlattices, *Nature* **579**, 359 (2020).
- [53] L. An, X. Cai, D. Pei, M. Huang, Z. Wu, Z. Zhou, J. Lin, Z. Ying, Z. Ye, X. Feng, *et al.*, Interaction effects and superconductivity signatures in twisted double-bilayer WSe_2 , *Nanoscale horizons* **5**, 1309 (2020).
- [54] S. Lisi, X. Lu, T. Benschop, T. A. de Jong, P. Stepanov, J. R. Duran, F. Margot, I. Cucchi, E. Cappelli, A. Hunter, *et al.*, Observation of flat bands in twisted bilayer graphene, *Nature Physics* **17**, 189 (2021).